ATLANTIS PRESS
Advances in Engineering Research (AER), volume 169
2nd International Conference on Material Science, Energy and Environmental Engineering (MSEEE 2018)

A Novel Metal-Free Visible-Light-Driven Photo catalytic Foam for Efficient Degradation of Methyl Orange

Junfeng Wu[1, a], Yan Gao[2, b] and Yi Li[3, c]

[1]Academy of Environmental Planning & Design, Co., Ltd, Nanjing University, Nanjing 210000, China.

[2]Jiangsu Engineering Consulting Center, Nanjing 210000, China.

[3]Hohai University, Nanjing 210000, China.

[a]jfwu@njuae.cn, [b]865780108@qq.com, [c]envly@hhu.edu.cn

Abstract. Here, graphitic carbon nitride (g-C_3N_4) was integrated with polyurethane foam (PUF) as a novel metal-free visible-light-driven photocatalytic foam (g-C_3N_4/PUF) by a facile ultrasonic method. The fabricated samples were characterized by scanning electron microscopy (SEM), transmission electron microscopy (TEM), X-ray Diffractometry (XRD) and UV-Vis diffuse reflectance spectroscopy (UV-V_{is} DRS). This composite foam exhibited enhanced photocatalytic performance compared to g-C_3N_4 powders for degradation of methyl orange (MO) in water without stirring under visible light irradiation. The pseudo-first order rate constant (kobs) for MO photodegradation by g-C_3N_4/PUF increased by up to a factor of 4.5 when compared with that of g-C3N4. The optimal addition dosage of g-C_3N_4 precursors for 1 cm^3 PUF was determined to be 0.5 g, namely g-C3N4/PUF-5. The new foam maintained its photocatalytic activity at least five consecutive cycles. Specially, the photocatalytic mechanism of g-C3N4/PUF was revealed, and superoxide radicals (•O_2-) were found to play a more dominant role than hydroxyl radicals (•OH) for organic pollutant degradation.

Keywords: Carbon nitride, polyurethane, floating, photocatalytic degradation.

1. Introduction

Photocatalytic oxidation is a promising technique to effectively decompose organic pollutants in water and wastewater *via* the generation of reactive oxygen species (ROS). Although TiO_2 semiconductor is the most widely investigated photocatalyst, it only works with UV activation that accounts for ~4% solar energy due to its wide band gap [1-3]. The ideal photocatalyst is supposed to be visible-light-responsive, highly effective, chemically stable, economically and environmentally feasible in engineering applications.

Recently, g-C_3N_4 attracts great interest for environmental applications [4] since it was first reported for photocatalytic water splitting under visible light irradiation [5]. This metal-free visible-light-active material can be simply and directly prepared from low cost nitrogen-rich precursors, namely heating the melamine [6, 7]. Unfortunately, a couple of bottlenecks for using powdered g-C_3N_4 in practical water purification are material aggregation and difficult separation.

Herein, we develop a novel metal-free visible-light-active photocatalytic foam by integrating g-C_3N_4 with PUF, namely g-C_3N_4/PUF, by a facile ultrasonic method. PUF was here chosen as the support because of its unique excellent properties, including open skeleton, high surface area, good flexibility and low density [8-10]. This photocatalytic foam can float on the upper surface of an aqueous reaction system, enhancing light utilization, ROS production, and thus photocatalytic degradation performance.

2. Experimental Section

2.1 Preparation of Photocatalytic Foams

The powdered photocatalyst of g-C_3N_4 was synthesized by directly heating melamine in the semi-closed system [6]. Typically, 10 g of melamine was placed into an alumina crucible with a cover. It was heated at a rate of 20 °C/min to 500 °C and then held for 2 h in a muffle furnace. Further, it was heated at 520 °C for another 2h. The obtained light-yellow powder was g-C_3N_4.

The floating photocatalyst of g-C_3N_4/PUF was synthesized by a facile ultrasonic method. An amount of 0.1, 0.3, 0.5 and 0.7 g of g-C_3N_4 was dispersed into 50 mL of methanol, respectively, and sonicated for 30 min. PUF (1 cm * 1 cm * 1 cm) was washed with ethanol and Milli-Q water for several times and dried at 60 ℃ for 30 min. After that, PUF was fully immersed into the g-C_3N_4 solution and sonicated at 60 ℃ for 60 min. Finally, the resulting foams were dried at 60 ℃ and donated as g-C_3N_4/PUF-1, g-C_3N_4/PUF-3 g-C_3N_4/PUF-5 and g-C_3N_4/PUF-7, respectively.

2.2 Photocatalytic MO Degradation

The photocatalytic degradation of MO by g-C_3N_4/PUF was carried out in a glass beaker irradiated by a 300 W Xenon lamp with a UV cut-off filter (visible light $\lambda \geq 400$ nm). In a typical photocatalytic experiment, the cube of g-C_3N_4/PUF was put in 50 mL of MO solution (5 mg/L). At certain time intervals of 30 min, the concentration of MO was measured by a UV-Vis spectrophotometer.

To investigate the photocatalytic mechanism of g-C_3N_4/PUF during photocatalytic degradation of MO, a series of experiments were conducted with the addition of individual scavengers. Briefly, 0.05 mmol/L of Cr(VI), 1 mmol/L of TEMPOL, and 0.5 mmol/L of isopropanol were added as scavengers for fully eliminating e^-, $\bullet O_2^-$, and •OH, respectively [11, 12].

3. Results and Discussion

SEM and TEM revealed that the morphology and microstructure of the freshly synthesized g-C_3N_4 powders were layer-like structures with irregular strips and patches (Figs. 1a and b). PUF was observed to possess well-defined macroporous networks (Fig. 1c), which can serve as an excellent support. Before loading, PUF exhibited a neat surface with the skeleton of 20 μm in width (Fig. 1d). As g-C_3N_4 was introduced onto PUF, the macroporous networks remained unchanged (Fig. 1e), and g-C_3N_4 was evenly distributed on the surface of PUF (Fig. 1f).

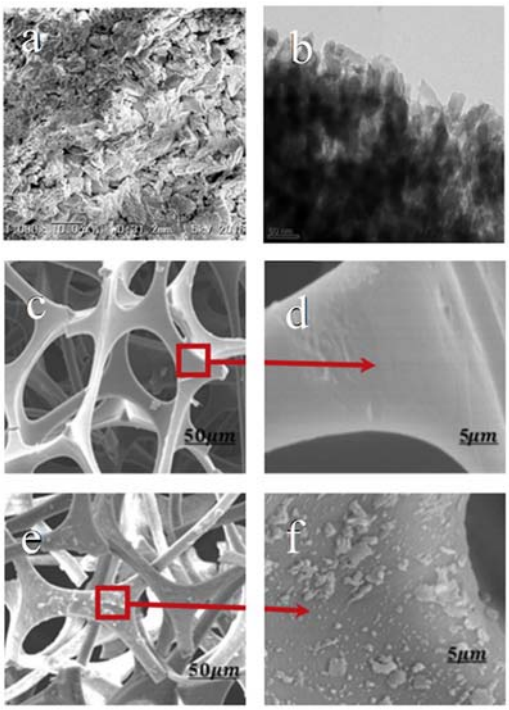

Fig. 1 A Typical (a) SEM Image and (b) TEM Image of g-C_3N_4, (c) SEM Image and (d) Magnified SEM Image of PUF, (e) SEM Image And (f) Magnified SEM Image of g-C_3N_4/PUF-5

XRD pattern of g-C_3N_4/PUF presented a typical dominant (002) diffraction peak at 27.6° with an interlayer distance of 0.33 nm (Fig. 2), which has been well known for g-C_3N_4 [13-15]. And a small (100) diffraction peak at 13.1° with an interlayer distance of 0.68 nm is attributed to the in-plane repeated units [16, 17].

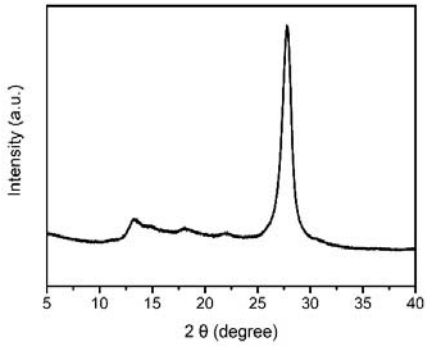

Fig. 2 XRD Pattern of g-C_3N_4/PUF-5

UV-Vis DRS spectrum of g-C_3N_4/PUF showed that this photocatalytic foam possessed a visible light absorption edge of ~450 nm (Fig. 3a). And its band gap energy was calculated to be ~2.75 eV according to the data of UV-Vis DRS (Fig. 3b), further proving that the prepared photocatalytic foam can absorb visible light.

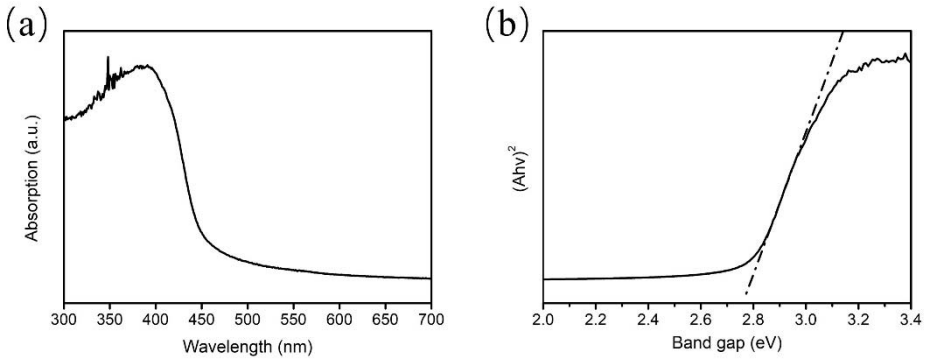

Fig. 3 UV-Vis DRS Spectrum (a) and Band Gap Calculation (b) of g-C_3N_4/PUF-5

Photocatalytic degradation of MO was performed by g-C_3N_4 powdered photocatalysts and g-C_3N_4/PUF floating photocatalysts without stirring under visible light irradiation (Fig. 4). Obviously, g-C_3N_4/PUF exhibited an enhanced photocatalytic activity for MO degradation compared with g-C_3N_4. During the photocatalytic reaction, MO could be completely removed by g-C_3N_4/PUF within 3 h, indicating g-C_3N_4/PUF is an efficient photocatalyst for organic pollutant degradation in water with reduced energy input.

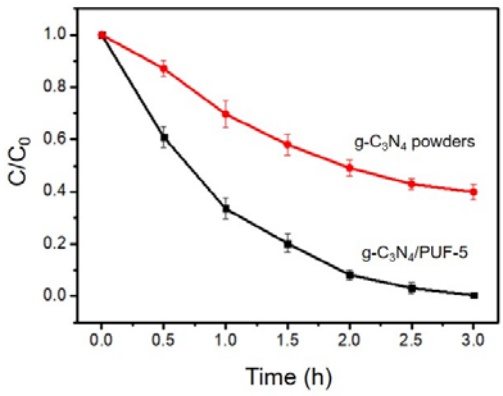

Fig. 4 Photodegradation of 5 mg/L MO by g-C_3N_4 Powders and g-C_3N_4/PUF-5 Foams without Stirring under Visible Light Irradiation.

A series of g-C_3N_4/PUF photocatalytic foams with different g-C_3N_4 loadings were used for MO degradation without stirring under visible light irradiation (Fig. 5). Along with the increasing of g-

C_3N_4 loadings in the composite, the MO degradation efficiency also increased due to the increased active sites in water [18, 19]. By further increasing g-C_3N_4 loadings in the composite, g-C_3N_4 could be aggregated, which decreased active sites and thus reduced the MO degradation efficiency. The g-C_3N_4/PUF-5 sample showed the highest photocatalytic activity which is related to the better dispersion of g-C_3N_4 over the PUF surface

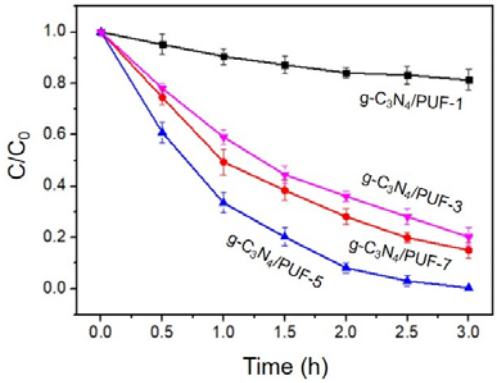

Fig. 5 Photodegradation of 5 mg/L MO by Different g-C_3N_4/PUF Samples without Stirring under Visible Light Irradiation

Moreover, the photocatalytic degradation of MO by g-C_3N_4/PUF followed the pseudo-first-order kinetics, and the k_{obs} for MO degradation changed upon changing g-C_3N_4 loadings in the composite. As shown in Table 1, the k_{obs} for MO degradation by g-C_3N_4 was 0.0051 min^{-1}. After loading on PUF, the k_{obs} for MO degradation increased from 0.011 min^{-1} for g-C_3N_4/PUF-1 to 0.0228 min^{-1} for g-C_3N_4/PUF-5. Further increasing g-C_3N_4 loading decreased the k_{obs} for MO degradation to 0.0087 min^{-1}, clearly showing that g-C_3N_4/PUF-5 among these g-C_3N_4 loadings is the optimal one to enhance the photocatalytic activity of g-C_3N_4/PUF in water without stirring under visible light irradiation.

Table 1. The Kobs for MO Photodegradation by Different g-C_3N_4/PUF Samples without Stirring under the Irradiation

Samples	g-C_3N_4	g-C_3N_4/PUF-1	g-C_3N_4/PUF-3	g-C_3N_4/PUF-5	g-C_3N_4/PUF-7
k_{obs} (min^{-1})	0.0051	0.0011	0.0106	0.0228	0.0087

The stability of a practical floating photocatalyst is as important as its photocatalytic activity [20]. The photocatalytic foam g-C_3N_4/PUF-5 was investigated through recycling experiments. As shown in Fig. 6, after five cycles of MO degradation, g-C_3N_4/PUF-5 did not show any significant loss of photocatalytic activity. These results indicate that the prepared g-C_3N_4/PUF-5 are an efficient and stable metal-free visible-light-driven photocatalytic foam, which can serve as a promising candidate for practical water purification with reduced energy input.

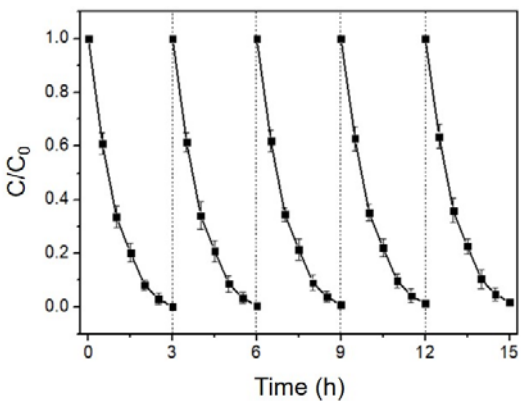

Fig. 6 Repeated Photocatalytic Degradation of MO by g-C_3N_4/PUF-5 without Stirring under Visible Light Irradiation

It has been found that the photocatalytic pollutant degradation is potentially caused by several main ROS produced from photocatalysts [21]. As shown in Fig. 7, after adding TEMPOL or isopropanol, the photocatalytic degradation efficiency of MO was significantly inhibited compared with no scavenger addition. This suggested that •O_2^- and •OH were the vital ROS in the photocatalytic system of g-C_3N_4/PUF. Importantly, •O_2^- were observed to play a more dominant role than •OH for MO degradation. Notably, the degree of inhibition caused by Cr (VI) was the highest, manifesting that the main ROS were generated in a reductive way from the conduction band of g-C_3N_4/PUF.

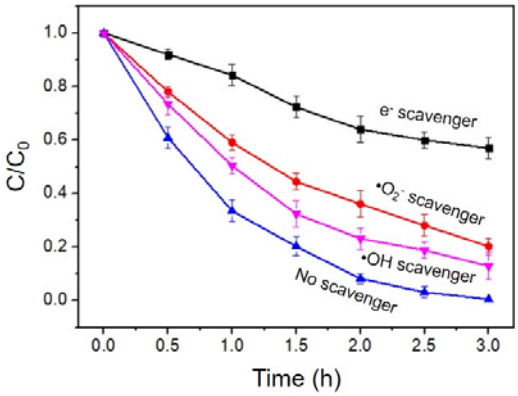

Fig. 7 Photocatalytic Degradation of MO by g-C_3N_4/PUF -5 with Different Scavengers under Visible Light Irradiation

4. Conclusion

In this study, we have synthesized g-C_3N_4/PUF for effective photocatalytic degradation of MO in water without stirring under visible light irradiation. The loading of g-C_3N_4 in the composite was found to influence the photocatalytic activity of this new photocatalytic foam, and an optimal one g-C_3N_4/PUF-5 was determined. The k_{obs} for photocatalytic MO degradation by g-C_3N_4/PUF-5 was up to 4.5 times higher than that of pure g-C_3N_4. The current photocatalytic foam is highly stable in use and its reusability up to 5 cycles has been examined. Both •O_2^- and •OH generated from g-C_3N_4/PUF-5 were revealed to be vital for MO degradation in water. This work opens an avenue for water purification with reduced energy input.

References

[1]. Zhang C, Li Y, Wang D, et al. Ag@ helical chiral TiO2 nanofibers for visible light photocatalytic degradation of 17α-ethinylestradiol. Environmental Science and Pollution Research. Vol. 22 (2015) No. 14, p. 10444-10451.

[2]. Pitre S P, Yoon T P, Scaiano J C. Titanium dioxide visible light photocatalysis: Surface association enables photocatalysis with visible light irradiation. Chemical Communications. Vol. 53 (2017) No. 31, p. 4335-4338.

[3]. Boningari T, Inturi S N R, Suidan M, et al. Novel one-step synthesis of sulfur doped-TiO2 by flame spray pyrolysis for visible light photocatalytic degradation of acetaldehyde. Chemical Engineering Journal. Vol. 339 (2018), p. 249-258.

[4]. Liu J, Liu Y, Liu N, Han, Y., et al. Metal-free efficient photocatalyst for stable visible water splitting via a two-electron pathway. Science. Vol. 347 (2015) No. 6225, p. 970-974.

[5]. Wang X, Maeda K, Thomas A, et al. A metal-free polymeric photocatalyst for hydrogen production from water under visible light. Nature Materials. Vol. 8 (2009) No. 1, p. 76-80.

[6]. Yan S C, Li Z S, Zou Z G. Photodegradation performance of g-C3N4 fabricated by directly heating melamine. Langmuir. Vol. 25 (2009) No. 17, p. 10397-10401.

[7]. Li Y, Zhang C, Shuai D, et al. Visible-light-driven photocatalytic inactivation of MS2 by metal-free g-C3N4: Virucidal performance and mechanism. Water Research. Vol. 106 (2016), p. 249-258.

[8]. Kumari S, Chauhan G S, Ahn J H. Novel cellulose nanowhiskers-based polyurethane foam for rapid and persistent removal of methylene blue from its aqueous solutions. Chemical Engineering Journal. Vol. 304 (2016), p. 728-736.

[9]. Qian X, Ren M, Yue D, et al. Mesoporous TiO2 films coated on carbon foam based on waste polyurethane for enhanced photocatalytic oxidation of VOCs. Applied Catalysis B: Environmental. Vol. 212 (2017), p. 1-6.

[10]. Wang S, Zhang Y, Dong F, et al. Readily attainable spongy foam photocatalyst for promising practical photocatalysis. Applied Catalysis B: Environmental. Vol. 208 (2017), p. 75-81.

[11]. Kumar A, Guo C, Sharma G, et al. Magnetically recoverable ZrO2/Fe3O4/chitosan nanomaterials for enhanced sunlight driven photoreduction of carcinogenic Cr(VI) and dechlorination & mineralization of 4-chlorophenol from simulated waste water. RSC Advances. Vol. 6 (2016) No.16, p. 13251-13263.

[12]. Liang J, Liu F, Li M, et al. Facile synthesis of magnetic Fe3O4@BiOI@AgI for water decontamination with visible light irradiation: Different mechanisms for different organic pollutants degradation and bacterial disinfection. Water Research, Vol. 137 (2018), p. 120-129.

[13]. Papailias I, Giannakopoulou T, Todorova N, et al. Effect of processing temperature on structure and photocatalytic properties of g-C3N4. Applied Surface Science. Vol. 358 (2015), p. 278-286.

[14]. Jo W K, Natarajan T S. Influence of TiO2 morphology on the photocatalytic efficiency of direct Z-scheme g-C3N4/TiO2 photocatalysts for isoniazid degradation. Chemical Engineering Journal. Vol. 281 (2015), p. 549-565.

[15]. Ma J, Yang Q, Wen Y, et al. Fe-g-C3N4/graphitized mesoporous carbon composite as an effective Fenton-like catalyst in a wide pH range. Applied Catalysis B: Environmental. Vol. 201 (2017), p. 232-240.

[16]. Akhundi A, Habibi-Yangjeh A. Codeposition of AgI and Ag2CrO4 on g-C3N4/Fe3O4 nanocomposite: Novel magnetically separable visible-light-driven photocatalysts with enhanced activity. Advanced Powder Technology. Vol. 27 (2016) No. 6, p. 2496-2506.

[17]. She X, Wu J, Xu H, et al. High efficiency photocatalytic water splitting using 2D α-Fe2O3/g-C3N4 Z-scheme catalysts. Advanced Energy Materials. Vol 7 (2017) No. 17, p. 1700025.

[18]. Song J, Wang X, Ma J, et al. Visible-light-driven in situ inactivation of Microcystis aeruginosa with the use of floating g-C3N4 heterojunction photocatalyst: Performance, mechanisms and implications. Applied Catalysis B: Environmental. Vol. 226 (2018), p. 83-92.

[19]. Zhang C, Li Y, Shuai D, et al. Visible-light-driven, water-surface-floating antimicrobials developed from graphitic carbon nitride and expanded perlite for water disinfection. Chemosphere, Vol. 208 (2018), p. 84-92.

[20]. Zhang C, Li Y, Zhang W, et al. Metal-free virucidal effects induced by g-C3N4 under visible light irradiation: Statistical analysis and parameter optimization. Chemosphere. Vol. 195 (2018), p. 551-558.

[21]. Oh W D, Lok L W, Veksha A, et al. Enhanced photocatalytic degradation of bisphenol A with Ag-decorated S-doped g-C3N4 under solar irradiation: Performance and mechanistic studies. Chemical Engineering Journal. Vol. 333 (2018), p. 739-749.